Earth Planet. Sci. Lett. 667 (2025) 119464

Contents lists available at ScienceDirect

Earth and Planetary Science Letters

journal homepage: www.elsevier.com/locate/epsl

The evolution of a Mid-Miocene geomagnetic reversal

Liz van Grinsven [a,*], Annemarieke Béguin [b], Klaudia F. Kuiper [c], Lennart V. de Groot [a]

[a] Paleomagnetic laboratory Fort Hoofddijk, Utrecht University, Budapestlaan 17, 3584 CD, Utrecht, the Netherlands
[b] Department of Geoscience and Petroleum, Norwegian University of Science and Technology, 7491 Trondheim, Norway
[c] Department of Earth Sciences, Vrije Universiteit Amsterdam, De Boelelaan 1085 1081,HV, Amsterdam

ARTICLE INFO

Editor: DR J BADRO.

Keywords:
Paleomagnetism
Geomagnetic reversal
Paleodirection
Paleointensity
Mid-Miocene
Gran Canaria

ABSTRACT

The Earth's magnetic field reverses its polarity non-periodically. Despite the large number of reversals in the magnetostratigraphic record, the geometry of the Earth's magnetic field and the mechanisms driving reversals are still largely enigmatic. On the one hand, this is because the more readily available sedimentary records lack temporal resolution to record the rapid field changes during a reversal, and on the other hand because the volcanic data records -that may have the necessary temporal resolution- are dependent on volcanic eruption frequency and much more difficult to find. Here we produce a geomagnetic record with high temporal resolution that formed during the shield-building phase on Gran Canaria, Spain. Furthermore, we provide five radio-isotope age constraints for the section containing a mid-Miocene geomagnetic reversal. Our full-vector geomagnetic record is one of the most detailed records of a reversal to date. Surprisingly, we find that in the most reliable part of our record of the reversal the declination reverses only once, while the inclination flips at least five times. Lastly, we interpret this record as a combination of a geocentric axial dipole and non-axial dipole fields and show that the contributions of the non-axial dipole field can be relatively strong.

1. Introduction

The Earth's magnetic field is on average over time a geocentric axial dipole (GAD), which is a magnetic field of a dipole aligned with the spin axis of the Earth. This magnetic field reverses its polarity non-periodically. During a reversal the Earth's magnetic field behaves chaotically; changes rapidly, has a low intensity and is no longer best described as a dipole field (e.g., Glatzmaier and Roberts, 1995). Despite the large number of reversals in the magnetostratigraphic record, the geometry of the Earth's magnetic field and the mechanisms driving reversals still remain enigmatic. This is partly due to the majority of reversal datasets in the record being sedimentary, which is often lacking temporal resolution for recording the rapid field changes during reversals (e.g., Langereis et al., 1992). The lesser available volcanic records may have the necessary temporal resolution. Volcanic records, however, describe a reversal in discrete steps and therefore often have insufficient transitional directions to characterize the geometry of the changing field well. The number of discovered volcanic records of a reversal with a sufficiently high number of transitional directions is limited (e.g., Herrero-Bevera and Valet, 1999; Coe et al., 2004), which greatly hinders furthering our understanding of geomagnetic reversals.

Leonhardt et al. (2002) and Leonhardt and Soffel (2002) discovered a volcanic record of a Mid-Miocene geomagnetic reversal with high temporal resolution on the island of Gran Canaria, Spain. They described the magnetic signal stored in this detailed volcanic record that is part of the Guigui formation and formed during the highly eruptive shield-building phase of the island. This section contains multiple polarity flips within presumably one reversal. The exact age and duration of this reversal were ambiguous since no radioisotope ages were obtained. Nevertheless, the paleomagnetic record has sufficient cooling units with a transitional direction to show the dynamic behavior of the field before and during the reversal. Here, we revisit this section to resample the cooling units of Leonhardt et al. (2002) and Leonhardt and Soffel (2002), and extend this section downwards, adding >600 m of stratigraphy. With rock magnetic measurements, paleodirection measurements and using the current state-of-the-art in paleointensity techniques we produce a new high resolution full-vector description of the geomagnetic field during this geomagnetic reversal. Moreover, we subjected five cooling units to a radiometric dating study producing $^{40}Ar/^{39}Ar$ ages to provide a new timeframe for this section. The resulting paleomagnetic record is one of the most detailed records of a reversal to date, shedding light on the dynamic behavior of the Earth's magnetic field during a reversal.

* Corresponding author.
E-mail address: l.b.vangrinsven@uu.nl (L. van Grinsven).

https://doi.org/10.1016/j.epsl.2025.119464
Received 23 April 2024; Received in revised form 28 April 2025; Accepted 21 May 2025
Available online 28 June 2025
0012-821X/© 2025 The Author(s). Published by Elsevier B.V. This is an open access article under the CC BY license (http://creativecommons.org/licenses/by/4.0/).

This is important for constraining geodynamo models that explain the behavior of the Earth's magnetic field by interaction between mantle heterogeneities and the motion in the fluid outer core.

2. Geological setting and sampling

Gran Canaria (28.0° N, 15.6° W) is part of the Canary archipelago, which is a group of intraplate volcanic islands, formed during the past 60 million years by the movement of the African plate over a long-lived stationary mantle plume (Carracedo, 1999). The oldest rocks on the island belong to the Guigui formation, formed during the shield building phase of the island, and are overlain by the Hogarzales formation (van den Boogaard and Schmincke, 1998). Previous geochronological work on these formations yielded ages of ~14.3 to 13.9 Ma for the Guigui formation and ~14.1 to 13.3 Ma for the Hogarzales formation (Abdel-Monem et al. (1971); McDougall and Schmincke (1976); Van den Boogaard and Schmincke (1998), Guillou et al. (2004)). More recent work assigns a somewhat older age to the short-lasting shield building phase of the island: 14.5–14.0 Ma (Troll and Carracedo, 2016). The section that we sampled belongs to the Guigui formation and consists of a thick sequence of lava flows of Hawaiian type fissure eruptions (Troll and Carracedo, 2016). Some microfaulting has been reported in the fieldwork area (Troll et al., 2002; Bellido-Mulas and Pineda-Velasco, 2008), but displacements are generally small, 10 to 20 m, with excesses up to 60 m. There is little to no vegetation in the fieldwork area; the stratigraphic control in the entire section is therefore very good and the occurrence of microfaults should be evident in the field.

We sampled 110 independent cooling units in this >900 m thick sequence of lava flows (Fig. 1). The individual cooling units were bracketed by (thin) layers of scoria. The 90 highest –and therefore youngest– of these cooling units were taken in four continuous sections (Fig. 2). These four sections start at 600 m above sea level and partly overlap with the section of Leonhardt et al. (2002). The lowest section (in blue in Figs. 1 and 2) comprises only three cooling units: GX1-GX3. Section 2 (in purple) are 12 cooling units: GR1-GR12; Section 3 (in yellow) 37 cooling units: GR13-GR49; and Section 4 (in orange) 38 cooling units: GR50-GR87. An observation platform, Mirador de San Nicolás (27.938° N, 15.761° W, Fig. 1), is located at the transition from Section 2 to 3. We extended this upper part of the section downwards and also sampled older cooling units along the road from Mirador de San Nicolás to the Ocean (GC-204 via Tasartico) at every ~50 m in elevation (in red in Figs. 1 and 2). This resulted in a total of 13 cooling units:

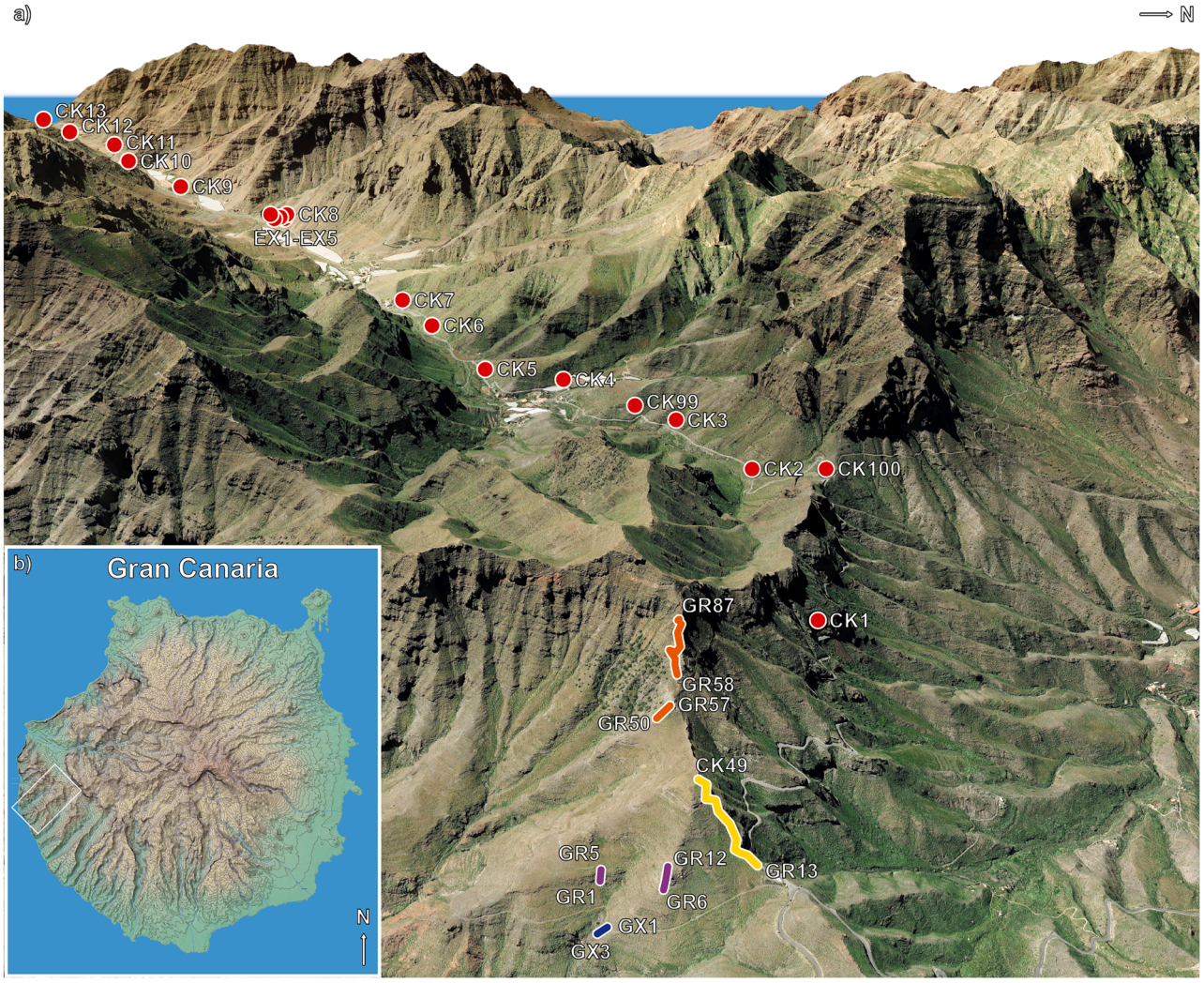


Fig. 1. Sampling locations on Gran Canaria, Spain. (a), birds eye view of the sampling locations on Gran Canaria, with the location on the island of Gran Canaria indicated in (b). The colored lines in a indicate continuous sampling of all cooling units, which correspond to the sections in Fig. 2: blue corresponds to cooling units GX3-GX1, purple to GR1-GR12, yellow to GR13-GR49 and orange to GR50-GR87. Below cooling unit GX3, a cooling unit was sampled approximately every 50 m in elevation downwards until sea level, corresponding to the red dots (sample code CK). An additional 5 cooling units were sampled surrounding cooling CK8.

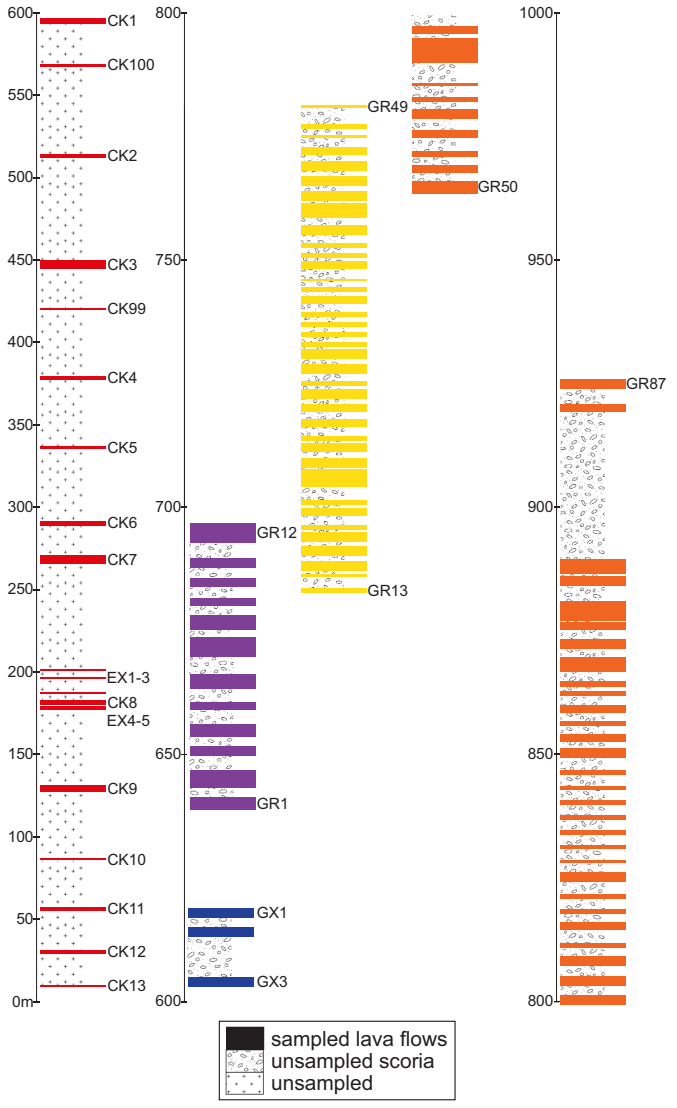


Fig. 2. Sampled cooling units. For every sampled cooling unit its elevation in meters above sea level and approximate thickness at the location of sampling is indicated by a colored bar, with colors corresponding to the sections in Fig. 1. In between the CK cooling units (red) the unsampled material contains cooling units and scoria, since the cooling units were sampled roughly every 50 m in elevation. The unsampled material in between the GX (blue) and GR (purple, yellow and orange) cooling units consist of scoria with no significant cooling units.

CK1-CK13, CK99 and CK100 (Fig. 1). Additional cooling units (EX1-EX5) were sampled around CK8, because of a potential microfault.

From each of the 110 cooling units, 8 to 12 samples were collected with a petrol-powered drill, from which at least 6 were oriented with a compass and, if possible, a sun compass. The samples within one cooling unit were taken at least 1 m apart and laterally well spread over the outcrop.

3. Methods

3.1. Rock magnetic characterization

To assess the characteristics of the samples as rock-magnetic recorders we measured their magnetic susceptibility as function of temperature with a AGICO KLY-3 kappabridge with a CS-3 furnace attachment. In addition, we measured the high-field behavior of the samples using a MicroSense Vibrating Sample Magnetometer (VSM).

The susceptibility as function of temperature measurements yields three pieces of information: first, the room temperature susceptibility; second, the dominant Curie temperature, which gives a first order assessment of the composition of the magnetic minerals; and third, the alteration temperature (T_{alt}), the temperature that can be reached without significantly changing the magnetic properties of the sample. For each cooling unit a crushed sample of approximately 0.75 g was heated in seven cycles with approximate peak temperatures of 180, 240, 300, 360, 420, 480 and 620 °C. After each peak temperature was reached, the temperature was lowered by 50 °C to test for alteration in the signal.

For each cooling unit one sample, with approximate dimensions of 0.5 × 0.5 × 0.5 cm, was measured on a MicroSense VSM. The Hysteresis and back-field curves obtained from the VSM were measured with a maximum applied field of 1.5 T We used the hysteresis loops and back-field curves to determine the saturation magnetization values (Ms), the remanent saturation magnetization values (Mr), the coercive field values (Bc) and the remanent coercive field values (Bcr).

3.2. Paleodirections

Paleomagnetic directions were obtained by both alternating field and thermal demagnetization experiments. A minimum of four samples per cooling unit were demagnetized by increasingly higher alternating fields using a robotized 2 G cryogenic magnetometer (Mullender et al., 2016), with peak fields of: 0, 2.5, 5, 7.5, 10, 15, 20, 25, 30, 40, 50, 60, 70, 80 and 100 mT. In addition, a minimum of 2 samples per cooling unit were thermally demagnetized using an ASC TD48-SC furnace with increasing steps of 50 °C until the sample was fully demagnetized. The samples were measured on a 2 G cryogenic magnetometer in between demagnetization steps. All demagnetization data was interpreted using Paleomagnetism.org (Koymans et al., 2016), which was also used to calculate the average direction of each cooling unit.

3.3. Paleointensities

Paleointensities were measured in two different ways: first with thermal IZZI-Thellier measurements yielding absolute estimates and second using pseudo-Thellier experiments that give a relative proxy of changes in paleointensity throughout the section.

Two samples from each cooling unit, except for EX1-EX3, were subjected to the IZZI-Thellier protocol (Tauxe and Staudigel, 2004; Yu et al., 2004) including pTRM checks (Coe, 1967), with a bias field of 40 μT. If the measurements of a cooling unit yielded interpretable results a further 4–5 samples were measured. The measurements were performed on the same equipment used for the thermal paleodirection experiments: a 2 G cyrogenic magnetometer and an ASC TD48-SC furnace. To optimize the thermal steps for the IZZI-Thellier experiments, the samples were divided into six different groups based on their rock magnetic analyses and thermal demagnetization behavior (de Groot et al., 2015). All results were analyzed using Paleointensity.org (Béguin et al., 2020). To exclude subjective bias while interpreting the data we used the automatic interpretation option. Following the interpretation protocol by de Groot et al. (2015), five predefined sets of selection criteria were used: TTA and TTB (Leonhardt et al., 2004) and SELCRIT2 (Biggin et al., 2007), as modified by Paterson et al. (2014); and Class A (de Groot et al., 2014) and CCRIT (Cromwell et al., 2015). Since CCRIT is the only set that addresses the curvature of the data, the curvature criteria ($|k'| <$ 0.35) was added to the other four sets, as this criterion is a strong indicator for multidomain behavior, and it reduces the scatter in the results (Paterson, 2011). All paleointensity results that passed one of the selection criteria were checked to remove all results that had clearly selected an overprint. The remaining paleointensity results were averaged per cooling unit, while interpretations that passed more than one set of criteria were weighted to the number of sets of criteria it passed.

Six samples from each cooling unit were subjected to pseudo-Thellier

paleointensity experiments (Tauxe et al., 1995; Yu et al., 2003; de Groot et al., 2013). The first step of this experiment is the alternating field demagnetization measurement which was also used for the paleomagnetic directions and described above. After this demagnetization measurement the same alternating field steps in combination with a bias field of 40 μT were used to impart partial anhysteretic remanent magnetizations (pARMS). These two measurements were analyzed using paleointensity.org (Béguin et al., 2020), and interpretations were only accepted if they pass the pTh-SCRIT selection criteria (Béguin et al., 2020). The pseudo-Thellier results are de facto the absolute slopes of the linear fit of the Arai plot, that are averaged for each cooling unit. In contradiction to the thermal paleointensity experiments, the resulting interpretations from the Pseudo-Thellier method give relative paleointensities. Therefore, these results first need to be scaled before they can be interpreted. Since the studied section contains a reversal, the paleointensities are expected to be low. For this reason, the method to convert pseudo-Thellier slopes in absolute paleointensities by de Groot et al. (2013) was not suitable, since it struggles with paleointensities below 20 μT (de Groot et al., 2013; 2015; 2016). Instead, the pseudo-Thellier results obtained here were pinpointed to the results of the IZZI-Thellier experiments, using the thermal paleointensity results as anchor points for the relative paleointensity curve. A scaling factor was calculated for the cooling units that gave a reliable thermal and pseudo-Thellier intensity result. The average of all these scaling factors was used to scale the entire pseudo-Thellier dataset.

3.4. Radioisotope dating

All paleomagnetic results were interpreted as function of elevation. To get an absolute estimate of the age of the reversal we performed $^{40}Ar/^{39}Ar$ datings for five levels in our stratigraphy: CK12 at 30 m, GR08 at 677 m, GR21 at 706 m, GR22 at 709 m, and GR80 at 868 m elevation. These samples were mainly chosen based on the absence of weathering in optical microscopy analysis and their spacing over the section. Samples from these five cooling units were crushed, washed and sieved in different size fractions. The 250–500 μm fractions were further separated using standard mineral separation procedures such as heavy liquid and magnetic separation to remove xenocyrsts. After a final handpicking step under an optical microscope, groundmass samples and standards were wrapped in Al-foil and irradiated for 7 h in the Oregon State University CLIICT Facility, USA (irradiation ID VU114). After irradiation, individual grains of standards were loaded in 2 mm diameter holes and bulk groundmass in 6 mm diameter holes of a Cu tray. This tray was prebaked for 24 h under vacuum at 250 °C and consecutively placed in the sample chamber connected to a Helix MC mass spectrometer and baked at 120 °C. A 25 W Synrad CO_2 laser is used for fusing the standards and incrementally heating the samples in 14 to 15 steps per sample. The released gas is purified using the Lauda cooler at 70 °C, a NP10 at 400 °C, ST172 at 400 °C and Ti sponge at 500 °C. The cleaned gas is expanded into a ThermoFisher Helix multi-collector mass spectrometer and ^{40}Ar is measured on the H2-Faraday cup, ^{39}Ar on the H1-CDD, ^{38}Ar on the AX-CDD, ^{37}Ar on the L1-CDD and ^{36}Ar on the L2-CDD (CDD = compact discrete dynode). All samples were measured in duplicate in March 2019. This was repeated in May 2019, so all samples were analyzed four times. The heating schedule is optimized based on data obtained from the first runs. A few heating steps in the first experiments are compromised by laser reflections heating surrounding holes. These results are reported but not included in data interpretation.

Data reduction was performed off-line using the ArArCalc software (Koppers, 2002) and the ages were calculated relative to Fish Canyon Tuff sanidine of 28.201 ± 0.022 Ma (Kuiper et al., 2008). Further details on the correction factors and errors are in Supplementary information 5. All relevant analytical data for age calculations can be found in Supplementary Figure 2.

4. Results

4.1. Rock magnetic characterization

The Rock magnetic characterization results, susceptibility and high field measurements, for one sample of each cooling unit are provided in Supplementary information. 1.

The room temperature susceptibility (Fig. 3a) is generally constant throughout the entire section, except for the cooling units in part C (677–712 m), which includes the overlap between the purple Section 2 and yellow Section 3. For these cooling units the room temperature susceptibility is markedly higher and more variable from one unit to another compared to other parts of the section. The Curie temperatures are generally high and indicate that magnetite is the dominant magnetic carrier for all cooling units. The alteration temperature is the highest temperature that shows reversable behavior and is an indication of the highest temperature that can be reliably interpreted in paleointensity experiments for that specific cooling unit.

With the parameters obtained from the high field measurements a Day plot (Day 1977) was created (Supplementary Figure 1), from which a first order interpretation of the magnetic bulk domain state of the sample was made by characterizing the sample as a Single Domain (SD), Multi Domain (MD) or Pseudo-Single Domain (PSD). Most samples are characterized by PSD behavior. Fifteen samples give Hcr/Hc values higher than four, which would classify them as MD, with two samples (GR15, 688 m and GR57, 792 m) giving a Mr/Ms values lower than 0.05 characterizing them as MD. Most of the cooling units with MD-like behavior in the Day-plot are in part C (677–712 m) – the same cooling units with a markedly higher room temperature susceptibility. Interestingly, these Fifteen cooling units with high Hcr/Hc values give a somewhat poorer paleomagnetic results, however, still three of these cooling units had successful IZZI-Thelier results and most of these sites gave reliable paleodirections.

4.2. Paleodirections

Paleodirections were obtained for all cooling units except GR44 (766 m). Fig. 4 presents two representative Zijderveld diagrams – one from thermal demagnetization and one from alternating field demagnetization – both from cooling unit GR75 (853 m). In both diagrams, overprints are observed in the lower demagnetization steps, followed by a relatively linear trend toward the origin in the higher demagnetization steps. Notably, sample GR75–6, subjected to alternating field demagnetized, remains partially magnetized even at the maximum applied field of 100 mT – a behavior observed in many of the alternating field measurements. The average Mean Angular Deviation angle for all interpreted Zijderveld diagrams is about 4°, indicating a generally well-defined paleodirectional signal. All the demagnetization data is accessible through MagIC and the average paleodirections, along with their uncertainties and quality parameters – all calculated by paleomagnetism.org (Koymans et al., 2016) - are also provided in Supplementary information 2. Additionally, paleodirections and their uncertainties are plotted as a function of elevation in Fig. 3b, c.

Almost all cooling units up to 600 m elevation show a declination and inclination that correspond to a reversed geomagnetic field. The exception is part A (180–201 m), with cooling unit CK8 and surrounding cooling units EX1-EX5, that have a close to normal polarity. Cooling units of part B (604–618 m), consisting of cooling units GX3-GX1 in the blue section, have a normal polarity. Their directions, however, do not agree with the highest cooling unit of the red CK section below, nor with the lowest cooling units of the purple Section 2 above it, which show a reversed direction. Where the sections overlap in part C (677–712 m) the declination and inclination are chaotic and could indicate rapid behavior of the geomagnetic field. The cooling units in this part that show (almost) normal polarity, however, are the bottom of the yellow Section 3, and the cooling units with a reversed polarity are the top of

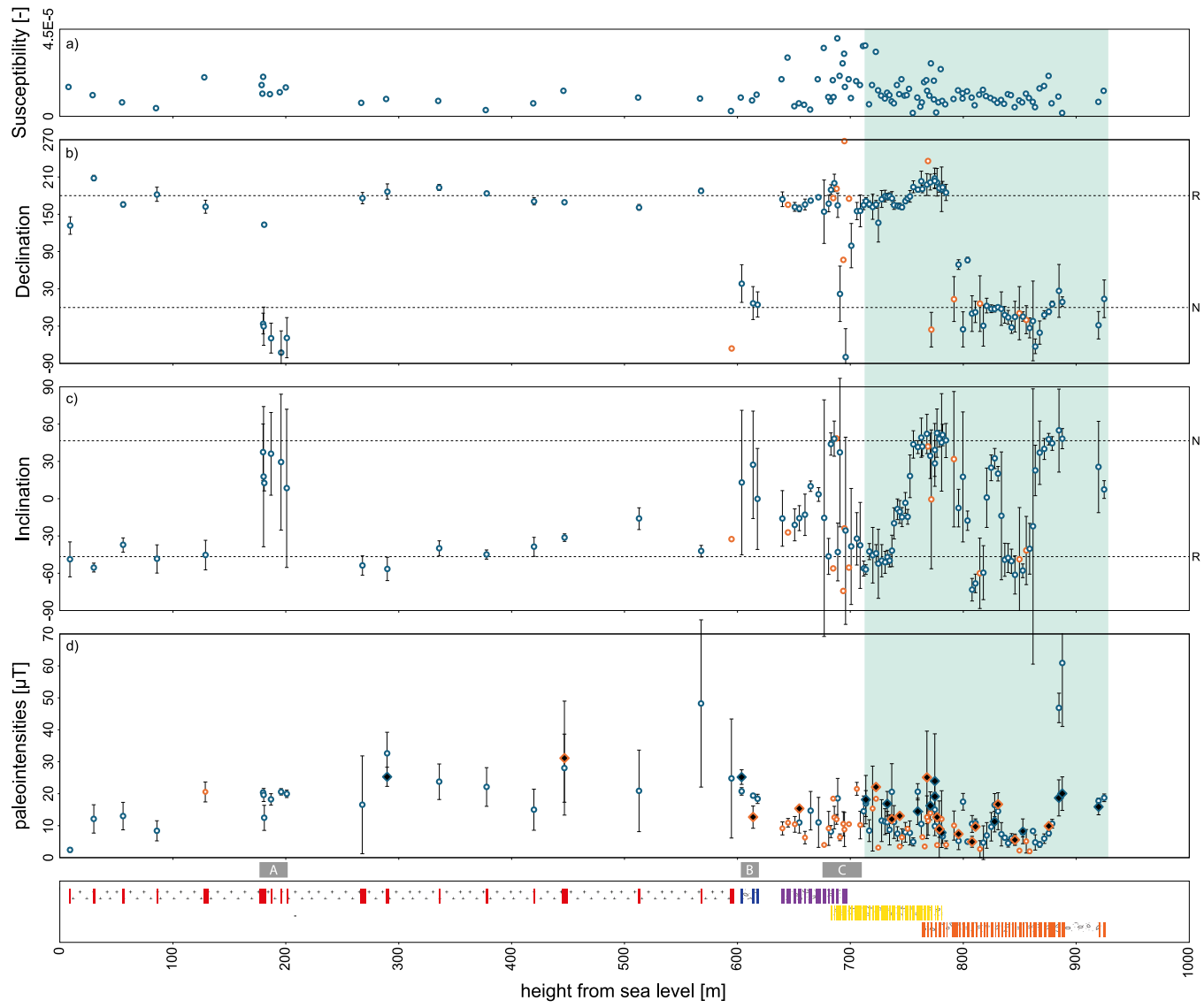


Fig. 3. Geomagnetic description of the Gran Canaria section. Every marker represents one cooling unit (corresponding to Fig. 2) and are plotted as function of elevation above sea level. The section and color codes are summarized at the bottom of the figure and Part A, B and C and the green shaded area mark sections that are discussed in the text. Panel a) contains the susceptibility at room temperature. The declination (b) and inclination (c) are given together with ΔD and ΔI uncertainty, and the colors of the markers indicate quality of the measurement, where a blue marker indicates a cooling unit with ≥4 samples and an uncertainty and an orange market indicates a cooling unit with ≤ 3 samples, or an cooling unit with such a low k value no ΔD and ΔI could be calculated. The declination and inclination that corresponds to the GAD-field for the latitude of Gran Canaria are indicated by dashed lines and index with 'N' for normal polarity and 'R' for reversed. The paleointensities are in panel d, with the diamond symbol representing the successful IZZI-Thellier measurements and the round symbol the scaled pseudo Thellier measurements. The error bars are the standard deviations of the Paleointensities for that cooling unit and the color of the symbol indicates the number of results on which the average for a cooling unit is based: blue is ≥4 samples and orange is ≤ 3.

the purple Section 2. In spite of the little vegetation, we cannot exclude the possibility that we did not correlate these two sections well or missed a microfault in between the purple Section 2 and the yellow Section 3. Also, the cooling units with most MD-like behavior in the Day plot, and highest susceptibility are from this interval, so this could also explain the lower quality of the paleomagnetic directions.

In the green shaded area (712–925 m), which consist of the top part of the yellow Sections 3 and the orange Section 4, the declination reversed only once to normal polarity, at 800 m, with three cooling units showing intermediate directions with declinations of 70 to 80° In contrast, the inclination in this part reversed polarity at least five times; from reversed to normal polarity at an elevation of 750 m, 820 m, and 860 m, and from reversed to normal polarity at an elevation of 800 m and 835 m. The section contains measurements up to 925 m elevation. There, the paleodirection shows a normal polarity and the reversal seems complete.

4.3. Paleointensities

All measurements of both the IZZI-Thellier and pseudo-Thellier experiments can be found on MagIC. Additionally, all cooling unit average paleointensities and their standard deviation are provided in Supplementary information 3 and are plotted in Fig. 3d.

The IZZI-Thellier experiments yielded absolute paleointensities for 29 of the cooling units, an example from GR75 (853 m) is in Fig. 4b. The IZZI-Thellier results differ in quality based on the number of samples per cooling unit that contributed to the cooling unit mean (denoted by color, Fig. 3d). 24 of the successful IZZI-Thellier results are from cooling units in the green shaded area (712–925 m). The absolute paleointensities indicate a relatively strong field (20–30 μT) below 600 m. Between 600

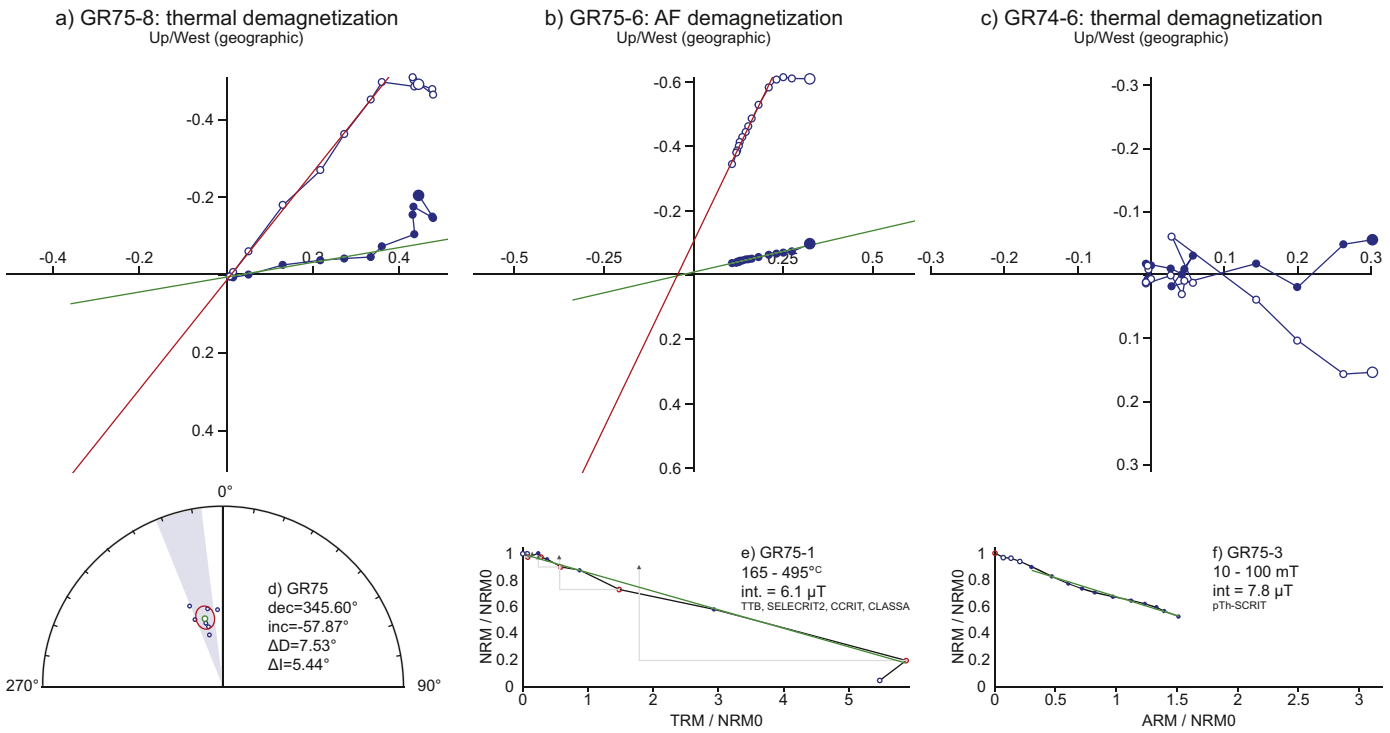


Fig. 4. Examples of paleomagnetic data. The paleomagnetic direction of cooling unit GR75 is typical for the quality of the results for the other cooling units, illustrated by a thermal (a) and alternating field (b) Zijderveld diagram [A/m] and an equal area projection of all the direction measurements of the cooling unit GR75 (d), with the *ΔD and ΔI uncertainty*. Some demagnetization experiments were unable to produce a reliable paleodirection, for instance GR74–6 (c). The IZZI-Thellier results for cooling unit GR75 is successful (e), with its results passing multiple sets of selection criteria (see main text). The pseudo-Thellier measurement for cooling unit GR75 yields a scaled paleointensity that compares well to the IZZI-Thellier result (f).

and 875 m the paleointensity fluctuates between 5 and 25 μT. Above 875 m the field seems to recover to 15 to 20 μT. During the geomagnetic reversal, we observe a pulsating field strength: it appears that the field is fluctuating between approximately 5 and 20 μT, with intensity peaks at 725, 775, 825 and 900 m elevation.

The Pseudo-Thellier experiments produced a relative paleointensity for 108 cooling units, which differ in quality depending on the number of samples per cooling unit that passed the selection criteria (denoted by color, Fig. 3d). The pseudo-Thellier were scaled to the IZZI-Thellier results by comparing the 14 cooling units that gave a reliable thermal and pseudo-Thellier intensity result, resulting in a scaling factor of -22.7. An example of a Pseudo-Thellier measurement of cooling unit GR75 (Fig. 4c), produces a paleointensity after scaling that is very similar to the IZZI-Thellier result. Results of the IZZI-Thellier and the Pseudo-Thellier measurements give similar results for most parts of the section, especially for the sequence from 600 to 900 m elevation. The exception in this upper part is the cooling units deposited after the last inclination flip at 885 m elevation, where the pseudo-Thellier data gives much higher paleointensities than the IZZI-Thellier data. These very high pseudo-Thellier paleointensities could be an artifact of the scaling of the pseudo-Thellier dataset, which is done with one factor for the entire dataset. The pulsating behavior found in the IZZI-Thellier data during the geomagnetic reversal is also found in the pseudo-Thellier data.

4.4. Radioisotope dating

All observed age spectra start with older apparent ages with lower radiogenic ^{40}Ar contents (low temperature steps). This is followed by a number of decreasing age steps in combination with increasing K/Ca ratios (decreasing K/Ca ratios for CK12, 30 m) and higher radiogenic ^{40}Ar* yields (~82–94 %) (intermediate temperature steps). All experiments end with a series of slightly younger age steps in combination with low K/Ca ratios and somewhat lower radiogenic ^{40}Ar* (~64–92 %) likely caused by degassing of plagioclase microphenocrysts within the groundmass.

Overall, initial high ages (generally the first 2–3 steps) with low ^{40}Ar* content may be the result of outgassing of alteration phases or low temperature excess argon. The intermediate temperature steps might be affected by ^{39}Ar recoil and the high temperature steps by ^{37}Ar recoil from Ca-bearing phases such as plagioclase (see Schaen et al., 2021 and references therein). Therefore, the age spectra do not meet nominal plateau criteria (Schaen et al., 2021), but can still be discussed within the context of other stratigraphic data. For all samples we report the total fusion age to compare to previous K-Ar studies, the weighted mean age of intermediate temperature steps and the weighted mean age of high temperatures steps. In all cases the scatter is higher than explained by analytical errors alone.

The samples from cooling units CK12 (30 m), GR21 (796 m), GR22 (709 m), and GR80 (868 m) yielded interpretable results. Although isochrons could not reliably be defined, there is no evidence for excess argon. If the intermediate steps are affected by ^{39}Ar recoil and the high temperature steps by ^{37}Ar recoil, we can interpret the high and intermediate temperature steps as upper and lower bounds, respectively (Table 1). This provides an age bracket of 15.2 to 14.0 Ma for the entire section (Fig. 5, Table 1). The sample from cooling unit GR08 (677 m) is the most altered sample we analyzed and should be treated with caution. Since its ages do not fit in the stratigraphic order compared to the other samples, we do not include this age in our interpretation.

Three interpreTable ^{40}Ar/^{39}Ar datings are stratigraphically between 700 and 900 m, the interval of our geomagnetic reversal, and yield interpretable ages (Fig. 5). When compared to the Geomagnetic Polarity

Table 1
Radioisotope ages. The calibrated $^{40}Ar/^{39}Ar$ ages are reported alongside their 2σ analytical uncertainties for the intermediate and high temperature steps, and their total external errors for the total fusion ages (see main text). The results of GR08 (677 m) should be treated with caution.

	intermediate temperature steps				high temperature steps				total fusion age		
	Age (Ma)	±2σ	$^{40}Ar^*$ (%)	K/Ca	Age (Ma)	±2σ	$^{40}Ar^*$ (%)	K/Ca	Age (Ma)	±2σ	K/Ca
CK12 - VU114-A1	15.21	0.21	82.5	0.22	14.42	0.14	69.4	0.05	15.22	0.32	0.13
GR08 - VU114-A5	*14.57*	*0.11*	*92.7*	*0.28*	*13.64*	*0.09*	*86.1*	*0.06*	*14.86*	*0.31*	*0.17*
GR21 - VU114-A2	14.82	0.11	90.3	0.32	14.12	0.13	64.2	0.05	14.95	0.31	0.18
GR22 - VU114-A3	14.78	0.09	93.9	0.30	13.99	0.06	92.0	0.07	14.84	0.31	0.17
GR80 - VU114-A4	14.80	0.08	85.1	0.28	14.32	0.05	75.1	0.06	14.80	0.31	0.13

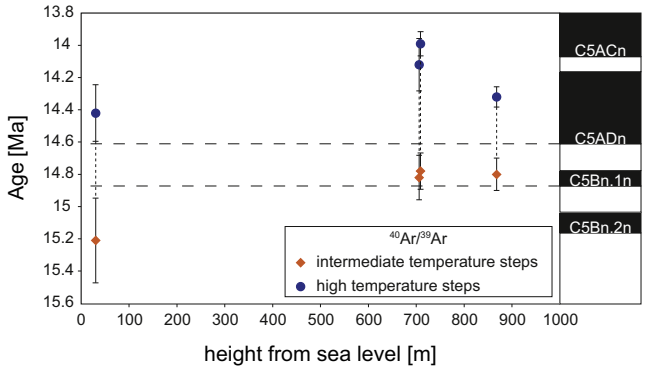


Fig. 5. Age of the Gran Canaria section. The four interpretable $^{40}Ar/^{39}Ar$ dates are plotted as function of their stratigraphic height, with the lower bounds defined by the intermediate temperature steps (orange diamonds) and the upper bounds given by the high temperature steps (blue circles). The geomagnetic polarity timescale (Ogg 2020) is on the right.

Timescale (Ogg, 2020), two transitions from reversed to normal polarity could agree with the age constraints obtained here: C5Bn.1r to C5Bn.1n at 14.870 Ma and C5ADr to C5ADn at 14.609 Ma. Given that the oldest option is almost at the end of the lower bound of the age bracket and just within uncertainty estimates, the latter option may be preferred, but our data is not conclusive between these two reversals.

5. Discussion

5.1. Geomagnetic records

Our record shows relatively stable magnetic recording properties throughout the section as illustrated by susceptibility and high-field measurement results. The success rate of paleointensity experiments is also high, especially in the section describing the geomagnetic reversal. Nevertheless, there are short parts of the stratigraphy that need some discussion; they are indicated with A, B, and C in Fig. 3.

In part A (180–201 m) we find a few cooling units with almost normal polarity, while the rest of the first 600 m of our record exhibits stable reversed polarity. The directions in part A, however, do not reach a fully reversed field (Fig. 3). We see three possibilities to explain this short period of almost normal polarity. First, it is possible that we missed a microfault in the field. The geology at this point is slightly less straightforward than elsewhere in the section since a major side-valley enters the main valley that we followed during our sampling just above part A. On the other hand, the geomagnetic directions that we find in multiple consecutive cooling units is close to a normal polarity, and not random. This makes a local tectonic event or disturbance not a likely candidate as this would have randomly reoriented the blocks. Second, the normal polarity in part A could be explained by a highly varying eruption frequency during the shield building phase of the island. In that case these cooling units could correlate to a chron of normal polarity preceding the geomagnetic reversal that is found higher in the stratigraphy. This is possible given our radioisotope age constraints (Fig. 5) but contradicts the indications of a constant eruption frequency by e.g., Van den Boogaard and Schmincke (1998) and Troll and Carracedo (2016). The two normal chrons that may be candidates, C5Bn.1n and C5Bn.2n, are 95 and 128 kyr long, respectively (Ogg, 2020). This implies that low in the stratigraphy approximately 25 m of stratigraphy corresponds to either 95 or 128 kyr, while only the reversal of the next chron would be captured by >200 m of stratigraphy. Since the paleomagnetic directions that we find in part A are also not fully reversed, we deem it unlikely that part A belongs to a preceding chron of normal polarity. Our third, and most likely explanation is that part A describes a short geomagnetic excursion during the chron of reversed polarity. This is supported by its short nature, the proposed constant eruption frequency during the shield building phase of the island, and by the fact that the paleomagnetic directions in part A do not fully reverse.

In the upper part of our record are two parts with lower data quality. First, part B (604–618 m) consist of only three cooling units that together form a small section of our stratigraphy. These three cooling units show a near-normal polarity, lacking intermediate directions before and after this section. It is unfortunate that the abrupt changes in the geomagnetic field coincide with these cooling units being a separate section in the stratigraphy; the cooling units directly above this section could not be sampled due to a road, and the cooling units below were inaccessible due to a steep cliff. Second, the cooling units from part C (677–712 m) show chaotic paleomagnetic directions and low quality paleointensity results. The cooling units from part C include an overlap of two section, where the top of the purple Section 2 yield almost reversed directions, while the cooling units at the bottom of the yellow Section 3 produce almost normal polarities. Although we did our best to correlate the different sections well in the field, it is very likely that an error in correlation was made. Remarkably, this overlap also corresponds to more variability in the rock-magnetic properties of the cooling units, as illustrated by the higher variation in susceptibility (Fig. 3a). This could be an explanation for the large uncertainties in measured paleodirections and very low IZZI-Thellier success rates. Due to the low data quality in part C and mismatch in sections, we choose to avoid the cooling units from part C in our further interpretation.

5.2. Age of the section

Our $^{40}Ar/^{39}Ar$ ages are slightly older (15.2 to 14.0 Ma) than the ages that were previously reported for the shield building phase of the island (14.5–14.0 Ma; Troll and Carracedo, 2016), and by geochronological work on the Guigui and Hogarzales formations (14.3 to 13.9 Ma and 14.1 to 13.3 Ma, respectively; Abdel-Monem et al., 1971; McDougall and Schmincke, 1976; Van den Boogaard and Schmincke, 1998; Guillou et al., 2004). These previous geochronological studies produced K-Ar ages, both on whole rocks and plagioclase. These published ages are summarized in Supplementary information 4 and were recalculated to the same set of decay constants as used in this study. For direct comparison of previous work with our work we also report our total fusion ages. We note that our total fusion ages are systematically older. This might suggest that not all $^{40}Ar^*$ is released in the K-Ar experiments yielding ages that are too young. Also, the complex behavior of the samples as seen in the age spectra will go unnoticed in K-Ar ages.

$^{40}Ar/^{39}Ar$ incremental heating experiments are therefore preferred. Our $^{40}Ar/^{39}Ar$ age constraints cannot discriminate whether the geomagnetic reversal in our record correspond to either one of two reversed to normal transitions in the magnetostratigraphic record: both the end of chron C5ADr at 14.870 Ma and C5Bn.1r at 14.609 Ma are within the uncertainties.

5.3. Duration of the reversal

In the top part of our record the declination flips polarity only once, at approximately 800 m above sea level. If we would consider only the declination, the geomagnetic reversal could be defined as a very short, almost instantaneous event. The inclination and intensity records, however, show a different picture. The inclination flips polarity five times in the interval between 735 and 875 m above sea level; and the intensity is markedly low between 640 and 880 m, although the onset of this period of low intensity is hampered by two less reliable intervals in our record (parts B and C in Fig. 3), and the end of this period is only defined by four cooling units at the very top of our section.

The two reversed to normal polarity transitions that could correspond to the geomagnetic reversal that we describe are the end of two reversed chrons with very similar duration: 162 kyr for C5ADr, and 166 kyr for C5Bn.1r (Ogg, 2020). Pinpointing the exact onset of the reversal in the record is difficult, also due to parts B and C with less certainty. There is a decrease in paleointensity already around 600 m above sea level, and the directions deviate from a reversed field for sure from 750 m onwards - most likely lower. This implies that 600 to 750 m of stratigraphy corresponds to at least 162 or 166 kyrs. This would correspond to a minimum average accumulation rate of 3.6 to 4.6 m/kyr. Since we did not find the start of the reversed chron below the geomagnetic reversal, it is likely that the chron is longer than our record. This would increase the calculated accumulation rates further. Given these accumulation rates, the period of switching inclinations from 735 to 875 m corresponds to 30.4 to 38.9 kyr. Again, this is an upper limit for the duration of the reversal itself and is critically dependent on the assumption of a constant eruption frequency for the entire section.

5.4. GAD vs NAD

Our paleomagnetic record of this mid-Miocene reversal is one of the most detailed records of a geomagnetic reversal to date. The record clearly indicates contributions of a NAD field, for instance with an inclination which reverses five times, whilst the declination only reverses once in the same timeframe. To further elaborate on this NAD field, we fitted a GAD (g_1^0) model to our intensity data. The paleomagnetic data used for this model is from the part of the record with the highest data quality: between 712 and 925 m (green shaded area in Fig. 3). For the model we use the directional and IZZI Thellier paleointensity data and omit the pseudo-Thellier data as this technique is less conventional to estimate the strength of the paleofield. First, a spline is fitted through the intensity data (Fig. 6c), to slightly smooth the data and to fill the data blanks in the record. With this spline the GAD term is calculated using the potential equation for the geomagnetic field (e.g., Tauxe, 2010).

To illustrate if the magnetic field direction is representing a GAD or NAD field, in other words if both the declination and inclination are showing the same polarity, Fig. 6 indicates whether the declination and inclination data are close to the value that corresponds with either a normal (pink shading) or reversed (yellow shading) polarity. If both the declination and inclination agree with either a normal or reversed polarity, the applicable shading is continued downwards in the panels of the measured and modeled intensity (Fig. 6c and d).

The studied section contains four intensity peaks at an elevation of approximately 725, 775, 825 and 900 m, that are labeled 1 to 4 in Fig. 6c. The two successful IZZI-Thellier results from the lower part of

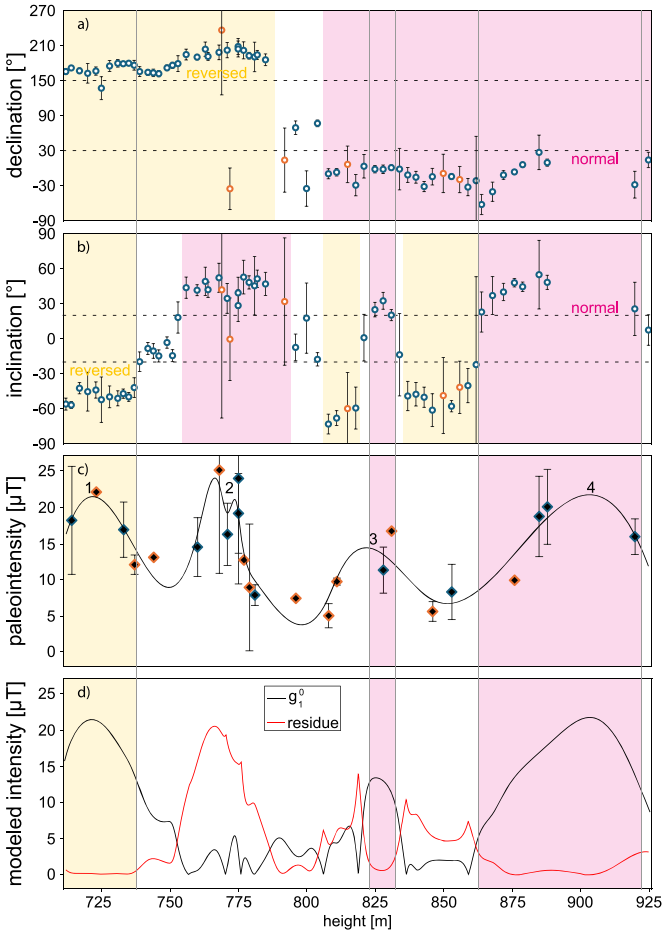


Fig. 6. The blue and orange markers with uncertainty in (a,b,c) contains the declination, inclination and IZZI-Thellier data points from Fig. 3, in the range of 712–935 elevation (green shaded area Fig. 3), which is the range with the highest data resolution. Through the paleointensity data points a spline is fitted, denoted by the black line. The data from this spline is used to fit a GAD (g_1^0) model to our intensity data, the intensity that can be fitted in this GAD component is shown by the black line in (d), the red line in (d) contains the residue unfitted intensity, in other words the black spline from (c) minus the black line of (d). The yellow and pink panels in (a,b) denote if the declination or inclination is reversed, yellow, or normal, pink, polarity. In (c) the yellow and pink panels are shown if both the declination and inclination are the same polarity. The numbers in (c) belong to the four intensity peaks within this part of the paleomagnetic record.

the stratigraphy leading up to the reversal (red section in Figs. 1 and 2) yielded 25.3 and 31.2 µT. The peaks during the reversal are thus almost as strong as the stable field during the reversed chron preceding the reversal.

Since our data for this reversal is spatially limited to this section, we could only fit the GAD term (g_1^0) to our data, the intensity of this GAD term is represented by the black line in Fig. 6d. The red line in this panel is the residual intensity from our data which was not fitted to the GAD term by our model. By definition, this residue must arise from the NAD field. The intensity of the fitted GAD term shows three peaks at approximately 725, 825 and 900 m elevation that coincide with the peak 1, 3, and 4 of our paleointensity data. This is expected, because during these peaks both the inclination and the declination show the same polarity. Surprisingly, during the second intensity peak, the field is in a NAD configuration with a declination close to reversed polarity and an inclination close to a normal configuration of the geomagnetic field. It is important to note that during this highly NAD configuration of the geomagnetic field, the observed field strength of the NAD component is

25 μT, or almost equal to the GAD field of the reversed chron leading up to the reversal. Even more interesting is the timing of this NAD peak: right before the only change in declination that we observe in this part of the record.

6. Comparison

The top 300 m of our sampled record was previously studied by Leonhardt et al. (2002) and Leonhardt and Soffel (2002) in Fig. 7, we compare their findings with our dataset. Both records exhibit similar magnetic field behavior, characterized by a single declination reversal and multiple inclination reversals. Additionally, both intensity records display a fluctuating pattern, with paleointensity highs of 25–30 μT and low between 1–5 μT.

Despite these overall similarities, the records do not align perfectly, likely due to differences in how the individual sections, both records were sampled from, were connected. Leonhardt et al. (2002) and Leonhardt and Soffel (2002) obtained their record from two sections with overlap between 760–800 m elevation, whereas our record includes overlapping intervals at 680–700 m and 760–780 m elevation. As noted previously, our data below 712 m elevation is less reliable due to uncertain stratigraphic correlation and low data quality. Within this interval, Leonahardt et al. (2002) and Leonhardt and Soffel (2002) report a stable declination, reversing inclination, and a generally decreasing paleointensity.

Between 712–925 m elevation, discrepancies remain, especially beyond 760 m, which likely stem from mismatches in section correlation, either in our own record or that of Leonhardt et al. (2002) and Leonhardt and Soffel (2002). Further refinement of stratigraphic alignment is necessary to resolve these inconsistencies.

This Mid-Miocene geomagnetic reversal is marked by a complex directional pattern, featuring multiple inclination flips and a single, distinct declination reversal. When compared to the classic precursor, transit and rebound model of geomagnetic reversals proposed by Valet et al. (2012), some similarities are evident. For instance, inclination reversals are observed in Leonhardt et al. (2002) and Leonhardt and Soffel (2002) at 630 m and 680 m elevation, and in our record at 610 m and 690 m elevation occurring prior to the declination reversal near 800 m in both records. Following this declination reversal, both records exhibit multiple inclination reversals until stabilizing into a normal polarity state around 900 m elevation. However, the reversal pattern captured in our record appears more complex than the simplified three-phase model alone can explain.

A particularly novel observation is the presence of a very strong NAD field, comparable in intensity to a stable GAD field, an unprecedented finding. While NAD dominance has been documented during reversals and excursion (e.g., Brown et al. 2018), such cases typically involve a weakened GAD component, allowing the NAD field to dominate. In

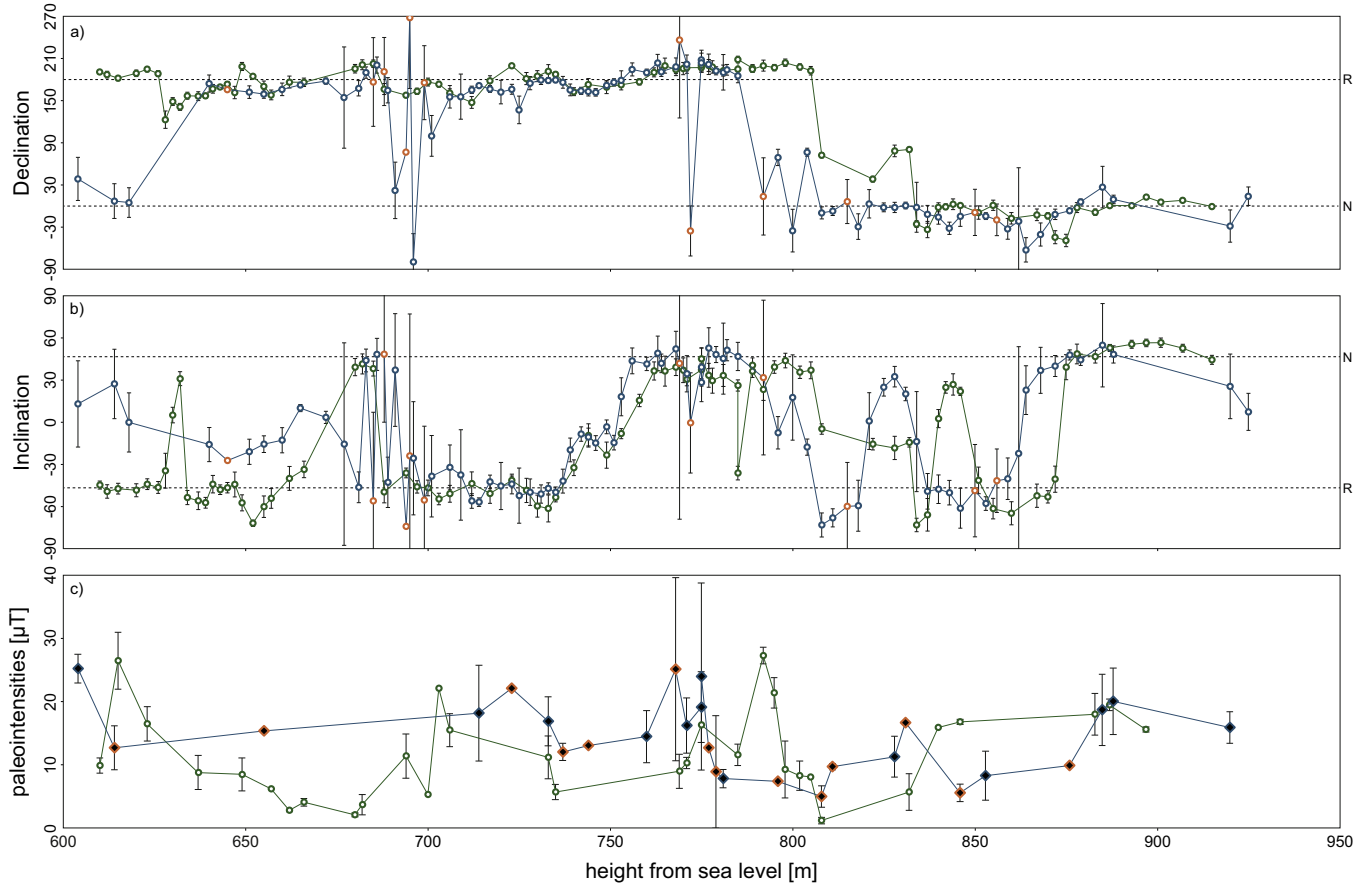


Fig. 7. Geomagnetic description of the top 300 m of our Gran Canaria section and the Gran Canaria section of Leonhardt et al. (2002) and Leonhardt and Soffel (2002). Every marker represents one cooling unit (corresponding to Fig. 2) and are plotted as function of elevation above sea level. The declination (a) and inclination (b) are given together with α95 uncertainty. The green markers represent the directions of Leonhard et al. (2002) and blue and orange markers are the directions obtained in this study, where the colors of the markers indicate quality of the measurement, a blue marker indicates a cooling unit with ≥4 samples and an uncertainty and an orange market indicates a cooling unit with ≤ 3 samples, or an cooling unit with such a low k value no ΔD and ΔI could be calculated. The declination and inclination that corresponds to the GAD-field for the latitude of Gran Canaria are indicated by dashed lines and index with 'N' for normal polarity and 'R' for reversed. The paleointensities are in panel c, with the green markers representing the paleointensity results from Leonhardt and Soffel (2002) and with the diamond symbol representing the IZZI-Thellier measurements from this study and the color of the symbol indicates the number of results on which the average for a cooling unit is based: blue is ≥4 samples and orange is ≤ 3. The error bars are the standard deviations of the Paleointensities for that cooling unit.

contrast, our data suggest a period of a genuinely strong NAD contribution. Additionally, the observation that field intensity does not remain consistently low throughout the reversal, but rather alternate between high and low values, is a new and noteworthy feature.

Lastly, while our estimates of reversal duration are not highly precise, they provide a valuable upper limit on the timeframe of most intense geomagnetic activity, approximately 30.4 to 38.9 kyr. These rough estimates also approach the upper end of previous reported reversal durations, including 7 kyr (Clement, 2004), 22 kyr (Singer et al., 2019), and 29 kyr (Mahgoub et al., 2023), reinforcing the relevance of our findings to the broader context of geomagnetic reversal research.

7. Conclusions

We produced a full-vector geomagnetic record of a Mid-Miocene reversal with a high temporal resolution. This temporal resolution enables interpreting the behavior of the geomagnetic field before and during a reversal. Four radioisotope datings provided temporal constraints, although the uncertainties prohibit discriminating between two possible geomagnetic reversals. The most reliable part of our geomagnetic record reveals only one transition from reversed to normal polarity in declination, while the inclination changes sign at least five times. Furthermore, we find that the intensity of the field is not necessarily extremely low during the reversal and seems to pulsate, with at least four peaks of more than half the present-day field strength for Gran Canaria. One of these peaks is a strong NAD feature, that is similar in strength to the other three peaks with a GAD signature. Our record of a geomagnetic reversal shows that current assumptions, e.g., that the field must be extremely weak, may not necessarily be true for local records of the geomagnetic reversal.

CRediT authorship contribution statement

Liz van Grinsven: Writing – original draft, Visualization, Software, Methodology, Investigation, Formal analysis, Data curation. **Annemarieke Béguin:** Methodology, Investigation, Formal analysis, Data curation. **Klaudia F. Kuiper:** Writing – review & editing, Writing – original draft, Methodology, Investigation, Formal analysis. **Lennart V. de Groot:** Writing – review & editing, Writing – original draft, Supervision, Funding acquisition, Data curation, Conceptualization.

Declaration of competing interest

The authors declare that they have no known competing financial interests or personal relationships that could have appeared to influence the work reported in this paper.

Acknowledgements

We thank Kira van Helden, Kari-Ann Marijnissen, Ana Nap, Katinka Tuinstra, and Silke van Klaveren for their help with sampling and data collection during their BSc theses. This project was funded by the Dutch Science Foundation (NWO) through VENI grant 863.15.003 and VIDI grant VI.Vidi.192.047 awarded to L.V.dG.

Supplementary materials

Supplementary material associated with this article can be found, in the online version, at doi:10.1016/j.epsl.2025.119464.

Data availability

Paleomagnetic data are available in the MagIC database (10.7288/V4/MAGIC/20370).

References

Abdel-Monem, A., Watkins, N.D., Gast, P.W., 1971. Potassium-argon ages, volcanic stratigraphy, and geomagnetic polarity history of the Canary Islands; Lanzarote, Fuerteventura, Gran Canaria, and La Gomera. Am. J. Sci. 271 (5), 490–521. https://doi.org/10.2475/ajs.271.5.490.

Béguin, A., Paterson, G.A., Biggin, A.J., de Groot, L.V., 2020. Paleointensity. org: an online, open source, application for the interpretation of paleointensity data. Geochem. Geophys. Geosyst. 21 (5), e2019GC008791. https://doi.org/10.1029/2019GC008791.

Bellido-Mulas, F., Pineda-Velasco, A., 2008. Mapa Geológico Digital continuo E. 1: 25.000, Zona Canarias-Gran Canaria.(Zona-2912). GEODE Mapa Geol. Digit. Contin. Esp.

Biggin, A.J., Perrin, M., Dekkers, M.J., 2007. A reliable absolute palaeointensity determination obtained from a non-ideal recorder. Earth Planet. Sci. Lett. 257 (3–4), 545–563. https://doi.org/10.1016/j.epsl.2007.03.017.

Brown, M., Korte, M., Holme, R., Wardinski, I., Gunnarson, S., 2018. Earth's magnetic field is probably not reversing. Proc. Natl. Acad. Sci. 115 (20), 5111–5116.

Carracedo, J.C., 1999. Growth, structure, instability and collapse of Canarian volcanoes and comparisons with Hawaiian volcanoes. J. Volcanol. Geotherm. Res. 94 (1–4), 1–19. https://doi.org/10.1016/S0377-0273(99)00095-5.

Clement, B.M., 2004. Dependence of the duration of geomagnetic polarity reversals on site latitude. Nature 428 (6983), 637–640.

Coe, R.S., 1967. The determination of paleo-intensities of the Earth's magnetic field with emphasis on mechanisms which could cause non-ideal behavior in Thellier's method. J. geomagn. geoelectr. 19 (3), 157–179. https://doi.org/10.5636/jgg.19.157.

Coe, R.S., Singer, B.S., Pringle, M.S., Zhao, X., 2004. Matuyama–Brunhes reversal and Kamikatsura event on Maui: paleomagnetic directions, 40Ar/39Ar ages and implications. Earth Planet. Sci. Lett. 222 (2), 667–684. https://doi.org/10.1016/j.epsl.2004.03.003.

Cromwell, G., Tauxe, L., Halldórsson, S.A., 2015. New paleointensity results from rapidly cooled Icelandic lavas: implications for Arctic geomagnetic field strength. J. Geophys. Res.: Solid Earth 120 (5), 2913–2934. https://doi.org/10.1002/2014JB011828.

Day, R., Fuller, M., Schmidt, V.A., 1977. Hysteresis properties of titanomagnetites: grain-size and compositional dependence. Phys. Earth Planet. Inter. 13 (4), 260–267. https://doi.org/10.1016/0031-9201(77)90108-X.

De Groot, L.V., Biggin, A.J., Dekkers, M.J., Langereis, C.G., Herrero-Bervera, E., 2013. Rapid regional perturbations to the recent global geomagnetic decay revealed by a new Hawaiian record. Nat. Commun. 4 (1), 2727. https://doi.org/10.1038/ncomms3727.

de Groot, L.V., Dekkers, M.J., Visscher, M., ter Maat, G.W., 2014. Magnetic properties and paleointensities as function of depth in a Hawaiian lava flow. Geochem. Geophys. Geosyst. 15 (4), 1096–1112. https://doi.org/10.1002/2013GC005094.

de Groot, L.V., Béguin, A., Kosters, M.E., van Rijsingen, E.M., Struijk, E.L., Biggin, A.J., Dekkers, M.J., 2015. High paleointensities for the Canary Islands constrain the Levant geomagnetic high. Earth Planet. Sci. Lett. 419, 154–167. https://doi.org/10.1016/j.epsl.2015.03.020.

de Groot, L.V., Pimentel, A., Di Chiara, A., 2016. The multimethod palaeointensity approach applied to volcanics from Terceira: full-vector geomagnetic data for the past 50 kyr. Geophys. J. Int. 206 (1), 590–604. https://doi.org/10.1093/gji/ggw095.

Glatzmaiers, G.A., Roberts, P.H., 1995. A three-dimensional self-consistent computer simulation of a geomagnetic field reversal. Nature 377 (6546), 203–209. https://doi.org/10.1038/377203a0.

Guillou, H., Torrado, F.J.P., Machin, A.R.H., Carracedo, J.C., Gimeno, D., 2004. The Plio–Quaternary volcanic evolution of Gran Canaria based on new K–Ar ages and magnetostratigraphy. J. Volcanol. Geotherm. Res. 135 (3), 221–246. https://doi.org/10.1016/j.jvolgeores.2004.03.003.

Herrero-Bervera, E., Valet, J.P., 1999. Paleosecular variation during sequential geomagnetic reversals from Hawaii. Earth Planet. Sci. Lett. 171 (1), 139–148. https://doi.org/10.1016/S0012-821X(99)00145-4.

Koppers, A.A., 2002. ArArCALC—software for 40Ar/39Ar age calculations. Comput. Geosci. 28 (5), 605–619. https://doi.org/10.1016/S0098-3004(01)00095-4.

Koymans, M.R., Langereis, C.G., Pastor-Galán, D., & van Hinsbergen, D.J. (2016). Paleomagnetism. org: an online multi-platform open source environment for paleomagnetic data analysis. DOI: 10.1016/j.cageo.2016.05.007.

Kuiper, K.F., Deino, A., Hilgen, F.J., Krijgsman, W., Renne, P.R., Wijbrans, A.J., 2008. Synchronizing rock clocks of Earth history. Science (1979) 320 (5875), 500–504. https://doi.org/10.1126/science.1154339.

Langereis, C.G., Van Hoof, A.A.M., Rochette, P., 1992. Longitudinal confinement of geomagnetic reversal paths as a possible sedimentary artefact. Nature 358 (6383), 226–230. https://doi.org/10.1038/358226a0.

Leonhardt, R., Matzka, J., Hufenbecher, F., Soffel, H.C., Heider, F., 2002. A reversal of the Earth's magnetic field recorded in mid-Miocene lava flows of Gran Canaria: paleodirections. J. Geophys. Res.: Solid Earth 107 (B1), EPM–EP7. https://doi.org/10.1029/2001JB000322.

Leonhardt, R., Soffel, H.C., 2002. A reversal of the Earth's magnetic field recorded in mid-Miocene lava flows of Gran Canaria: paleointensities. J. Geophys. Res.: Solid Earth 107 (B11), EPM–EP5. https://doi.org/10.1029/2001JB000949.

Leonhardt, R., Heunemann, C., Krasa, D., 2004. Analyzing absolute paleointensity determinations: acceptance criteria and the software ThellierTool4. 0. Geochem. Geophys. Geosyst. 5 (12). https://doi.org/10.1029/2004GC000807.

Mahgoub, A.N., Korte, M., Panovska, S., 2023. Global geomagnetic field evolution from 900 to 700 ka including the Matuyama-Brunhes reversal. J. Geophys. Res.: Solid Earth 128 (6), e2023JB026593.

McDougall, I., Schmincke, H.U., 1976. Geochronology of Gran Canaria, Canary Islands: age of shield building volcanism and other magmatic phases. Bull. Volcanol. 40, 57–77. https://doi.org/10.1007/BF02599829.

Mullender, T.A., Frederichs, T., Hilgenfeldt, C., de Groot, L.V., Fabian, K., Dekkers, M.J., 2016. Automated paleomagnetic and rock magnetic data acquisition with an in-line horizontal "2 G" system. Geochem. Geophys. Geosyst. 17 (9), 3546–3559. https://doi.org/10.1002/2016GC006436.

Ogg, J.G., 2020. Geomagnetic polarity time scale. Geologic Time Scale 2020. Elsevier, pp. 159–192. https://doi.org/10.1016/B978-0-12-824360-2.00005-X.

Paterson, G.A., 2011. A simple test for the presence of multidomain behavior during paleointensity experiments. J. Geophys. Res.: Solid Earth 116 (B10).

Paterson, G.A., Tauxe, L., Biggin, A.J., Shaar, R., Jonestrask, L.C., 2014. On improving the selection of Thellier-type paleointensity data. Geochem. Geophys. Geosyst. 4, 1180–1192. https://doi.org/10.1002/2013GC005135.

Schaen, A.J., Jicha, B.R., Hodges, K.V., Vermeesch, P., Stelten, M.E., Mercer, C.M., Singer, B.S., 2021. Interpreting and reporting 40Ar/39Ar geochronologic data. GSA Bull. 133 (3–4), 461–487. https://doi.org/10.1130/B35560.1.

Singer, B.S., Jicha, B.R., Mochizuki, N., Coe, R.S., 2019. Synchronizing volcanic, sedimentary, and ice core records of Earth's last magnetic polarity reversal. Sci. Adv. 5 (8), eaaw4621.

Tauxe, L., 2010. Essentials of Paleomagnetism. Univ of California Press.

Tauxe, L., Pick, T., Kok, Y.S., 1995. Relative paleointensity in sediments: a pseudo-Thellier approach. Geophys. Res. Lett. 22 (21), 2885–2888. https://doi.org/10.1029/95GL03166.

Tauxe, L., Staudigel, H., 2004. Strength of the geomagnetic field in the Cretaceous Normal Superchron: new data from submarine basaltic glass of the Troodos Ophiolite. Geochem. Geophys. Geosyst. 5 (2). https://doi.org/10.1029/2003GC000635.

Troll, V.R, Carracedo, J.C., 2016. The Geology of the Canary Islands. Elsevier. https://doi.org/10.1130/0091-7613(2002)030<0135:CCCPOP>2.0.CO;2. 10.5194/se-3-97-2012.

Troll, V.R., Walter, T.R., Schmincke, H.U., 2002. Cyclic caldera collapse: piston or piecemeal subsidence? Field and experimental evidence. Geology. 30 (2), 135–138.

Valet, J.P., Fournier, A., Courtillot, V., Herrero-Bervera, E., 2012. Dynamical similarity of geomagnetic field reversals. Nature 490 (7418), 89–93.

van den Bogaard, P., Schmincke, H.U., 1998. Chronostratigraphy of Gran Canaria. Proc. Ocean Drill. Program: Sci. Results 157 (Chapter 11), 127–140. https://doi.org/10.2973/odp.proc.sr.157.116.1998.

Yu, Y., Dunlop, D.J., Özdemir, Ö., 2003. Are ARM and TRM analogs? Thellier analysis of ARM and pseudo-Thellier analysis of TRM. Earth Planet. Sci. Lett. 205 (3–4), 325–336. https://doi.org/10.1016/S0012-821X(02)01060-9.

Yu, Y., Tauxe, L., Genevey, A., 2004. Toward an optimal geomagnetic field intensity determination technique. Geochem. Geophys. Geosyst. 5 (2). https://doi.org/10.1029/2003GC000630.